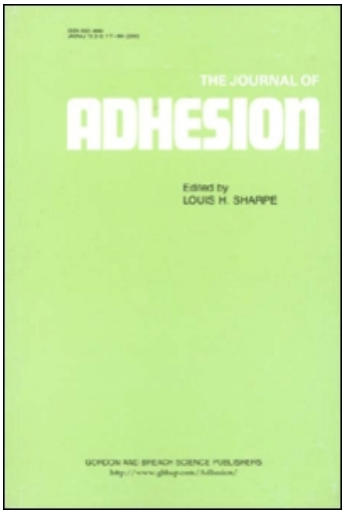

The Journal of Adhesion
Publication details, including instructions for authors and subscription information:
http://www.informaworld.com/smpp/title~content=t713453635

Highly Predictive Structural Cell for Particulate Polymeric Composites

V. V. Moshev[a]; L. L. Kozhevnikova[a]
[a] Institute of Continuous Media Mechanics, Russian Academy of Sciences, Perm, Russia

To cite this Article Moshev, V. V. and Kozhevnikova, L. L.(1997) 'Highly Predictive Structural Cell for Particulate Polymeric Composites', The Journal of Adhesion, 62: 1, 169 — 186
To link to this Article: DOI: 10.1080/00218469708014568
URL: http://dx.doi.org/10.1080/00218469708014568

J. Adhesion, 1997, Vol. 62, pp. 169–186
Reprints available directly from the publisher
Photocopying permitted by license only

Highly Predictive Structural Cell for Particulate Polymeric Composites

V. V. MOSHEV and L. L. KOZHEVNIKOVA

Institute of Continuous Media Mechanics, Russian Academy of Sciences, Korolev Str. 1, 614061, Perm, Russia

(Received 11 May 1996; In final form 18 November 1996)

A unit cell of a specified shape under specified loading conditions has been offered for predicting some basic properties of particulate polymeric composites. The stress-strain state of the bonded and debonded cell has been calculated in the framework of the large deformation approach within a wide range of filler volume concentrations. Effective modulus-filler concentration curves have been predicted on the basis of the unique cell investigation for bonded and debonded cell states and have proved to be in good agreement with the available experimental data. Local strain concentration as a function of cell extension and filler volume loading has been estimated.

Keywords: Polymeric particulate composites; cell model; matrix-filler debonding; large deformation theory; boundary value problem; finite element method

1 INTRODUCTION

The choice of the form and loading conditions for structural elements is, possibly, the most important stage in searching for an adequate simulation of particulate composite behavior, when the study is aimed both at an understanding of micromechanisms of deformation and at effective properties evaluation.

A great number of structural cell models have been offered for particulate systems. Some of them represent one particle simulation [1–3] aimed at investigation of special micro-mechanical problems. Other approaches emerge from the structural elements being regarded as certain phenomenological objects with a specified set of properties. They are usually focused on averaging problems [4–6]. In suspension mechanics, a model has been offered based on a consideration of a

unit structural cell surrounded by adjacent neighbors [7]. As far as we know, these studies were made in the framework of linear mechanics. In Reference [8], a cell model has been suggested that has taken into consideration the peculiarities pertinent to large deformation. However, this approach did not account for the restrained conditions inherent in real particulate composites.

In this paper we examine a rather simple one-particle structural unit cell that, in our opinion, is more predictive as compared with the others of the same nature from both the micro- and macromechanical points of view. The high efficiency of such a cell is reached due to the appropriately chosen geometrical shape and to the specified boundary conditions. Simple extension including the interface separation and final failure is examined.

2 THEORETICAL BACKGROUND

2.1 Model Cell Geometry and Boundary Conditions

In Reference [8], a unit cell has been offered having the form of a cylinder (matrix) with a rigid spherical inclusion (filler particle) placed at the center, the height of the cylinder being taken equal to its diameter. The cell has been tested in simple tension. The cylinder ends were moved apart, vertical displacements being constant and the radials ones not being constrained. No stresses were imposed on the lateral part of the cylinder. Calculations performed subsequently have shown that cells with a non-restricted lateral boundary underestimate the effective rigidities of the cells as compared with real materials.

If one looks at the unit cell as an element within a closely packed ensemble shown in Figure 1, it becomes obvious that the lines of contact between the adjacent cells must remain straight during extension, to keep the continuity of the system. Such boundary displacements together with the cell's ends remaining flat seem to define more adequately the state of the cell during its extension.

So, the features pertinent to the current calculations have been finally chosen as follows: (1) constant vertical displacements of the cell ends have been imposed with the radial ones not restrained; (2) constant radial displacements over the lateral boundary have been postulated

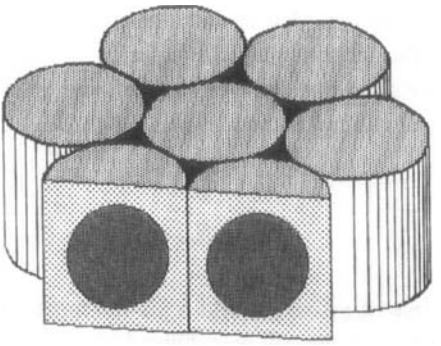

FIGURE 1 Packing of model cells.

with the force vector equal to zero, implying the absence of lateral pressure during extension.

The geometry offered is characterized by another remarkable feature. Having increased the radius of the spherical inclusion until it touches the lateral boundary of the cell, we come the maximum filler volume (inside the ensemble of particles) equal to 0.607 which is very close to that characterizing the ultimate packing of random structures composed of the uniformly-sized spheres [9–11]. This agreement urged us to anticipate that the properties of the unit cell in question would be, possibly, able to reflect rather adequately the concentration behavior of particulate composites.

A constant value, namely 2 cm, has been assigned to the diameter and height of the cell. The diameter of the inclusion has been adopted as a varying parameter that allowed the imposition of different filler concentrations. These have been expressed as the ratio of the volume of the inclusion to the volume of the cylinder.

2.2 Modeling Conditions

The cell was tested in simple tension, the cylinder ends being moved apart. In all instances, the life cycle of the cell started from the unstressed state with the inclusion bonded to the matrix. During extension, the detachment of the matrix from the inclusion occurred with the appearance of a pore having the form of the vacuole. No surface tractions were applied to the surface of the detached portion of the

vacuole. The cell was regarded as having failed when the maximum deformations of the matrix near the equatorial part of the sphere reached some ultimate value characteristic of pure gum vulcanizate.

The resistance of the model was expressed through reduced stress, σ, defined as

$$\sigma = F/S_0,$$

where F is the force of extension and S_0 is the initial cross-section of the cell. The strain, ε, of the cell was defined as

$$\varepsilon = \Delta H/H,$$

where ΔH is the extension of the ends and H is the height of the cell.

In all the numerical experiments the maximum straining of the model was bounded by 50 per cent.

2.3 Mechanical Properties of Constituent Materials and Matrix Debonding Conditions

The approach adopted is purely an elastic one, only an equilibrium time-independent process being examined. The matrix phase is represented by an incompressible elastomer following the neo-Hookean behavior characterized by one material parameter, C,

$$W = C(I_1 - 3) \tag{1}$$

where W is the elastic potential, I_1 is the first main invariant of the Cauchy-Green deformation tensor, C is a constant whose value is taken equal to 0.05 MPa, which corresponds to the Young's modulus of 0.3 MPa within the range of small deformations.

Generally, this approach may be used for any elastic matrix with the specified elastic potential.

The solid sphere is taken to be perfectly rigid, all the energy of deformation thus being stored within the matrix volume.

To describe the origination and progression of the debond, Griffith's approach has been used in much the same way as has been done

in other publications [12–14], where the postulates of the existence of small precursor debonds and the invariance of debond energy during crack growth have been adopted.

It will be shown later on that the most probable point of the postulated debond is positioned at the inclusion's pole zone, where maximum strains and hydrostatic extensions are concentrated.

The energy, T_d, required for further matrix detachment has been defined as

$$T_d = (dW/dS), \tag{2}$$

where dW is the energy increment of our system needed to increase the crack area by dS, T_d being the characteristic property of the pair "matrix-inclusion" regarded as the cohesive or adhesive tear energy.

The only energy source for debonding is the current strain energy, W, accumulated in the matrix. That depends both on the current cell extension, ε, and on the current crack area, S

$$W = \phi(\varepsilon, S).$$

The condition (2) may now rewritten as

$$T_d = d(\phi(\varepsilon, S))/dS = \psi(\varepsilon, S). \tag{3}$$

Having assumed T_d to be some characteristic property of the cell system and having assumed its value to remain constant during the entire process of the matrix detachment from the inclusion, we open the opportunity to establish an explicit interrelation between ε and S by means of Equation (3). For a number of growing S_i values, beginning with the small initial one, corresponding ε_i values are calculated through Equation (3). Remembering that the resistance of the cell, F, is also defined by the current values of ε and S, the $F \sim \varepsilon$ relation characterizing tensile behavior under the imposed T_d can be obtained.

Hence, the process of debonding may be regarded as that of the transfer of the cell from the initial state of a nearly-perfect bond to the final one of complete separation.

The tear strength of the elastomer, T_e, may be considered as a magnitude that provides the ultimate bond strength. Lesser energies of

debonding can be judged as magnitudes characterizing the filler-matrix strength of adhesion.

According to Gent and Tobias [14] the threshold tear strength of a hydrocarbon elastomer correlates with its Young's modulus. The use of this correlation has permitted us to specify the threshold tear strength for the matrix in this paper at the level of 150 J/m^2.

In consequent calculations, T_d values are taken equal to 150 J/m^2 or some lesser values simulating adhesive debond behavior.

2.4 Calculation Procedure

The features of the calculation method are published elsewhere [15]. Briefly, the method consists in using a function,

$$He(H,\bar{u}) = \int_{V_0} (AH(I_3 - 1) - A^2(\alpha/2)(H - \chi^*)^2 + W(I_1, I_2) + 0.5(k_1 + k_2)((I_3 - 1) - A\alpha(H - \chi^*))^2 - \rho^0 \bar{K}\bar{u})\, dV_0 - \int_{S_p^0} \bar{p}\bar{u}\, {}_\alpha S_p^0$$

Here, A and α are generalized elastic moduli, k_1 and k_2 being the coefficients for C (Eq. (1)) expansion in series; $\bar{u}$ is the displacement vector; V_0 and S_p^0 are, respectively, the unstrained volume with volume forces, $\bar{K}$, and density, ρ^0, and the surface, where forces, $\bar{p}$, are applied. For an incompressible material, the generalized modulus of elasticity, α, is equal to zero. Then the incompressibility condition $(I_3 - 1)$ is satisfied automatically during variation of the function with H. The function is varied in H and $\bar{u}$. Minimizing $He(H,\bar{u})$ on $\bar{u}$ and H produces a set of variational equations to all the differential equations of continuum mechanics.

The finite element method was used for calculations. A typical sketch of the adopted finite element grid is shown in Figure 2 for a solid volume fraction of 40%. Considering the geometry of the cell, a condensation of elements near the inclusion was performed.

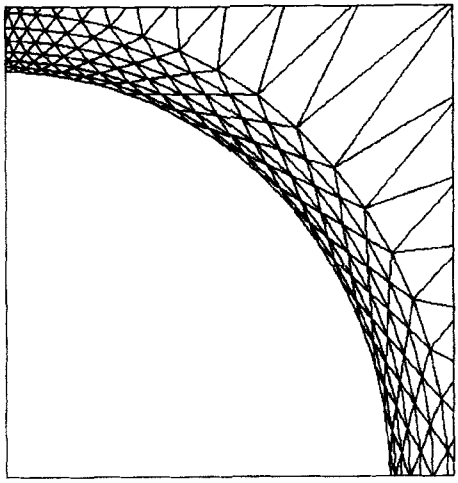

FIGURE 2 Finite element grid adopted for calculations.

Displacement vector components and mean stress function in n and m nodes were approximated by the shape function Ψ_p and ϕ_N. Then, the displacements are $\boldsymbol{u}_p = \boldsymbol{\psi}_p \boldsymbol{u}_p^n$, and $\boldsymbol{u}^k = \boldsymbol{\psi}_m \boldsymbol{u}^{mk}$, while the mean stress function $\boldsymbol{H} = \boldsymbol{\psi}_N \boldsymbol{H}^N$. Here, $\boldsymbol{u}_p^n$, $\boldsymbol{u}^{mk}$ are covariant and contravariant displacement vector components.

A program was developed for the incremental load procedure, using triangular cylindrical finite elements with a square approximation to the displacement field, and linear functions for the mean pressure. In contact zones, the conditions for non-penetration and non-positiveness of normal pressure, were introduced.

The initial small debond, in the form of disconnected matrix nodes at the poles and at their nearest interfacial neighbors, was introduced to make feasible the Griffith's approach. The area of such a debond was only about 1% of the total interface area. The calculations have shown that $F \sim \varepsilon$ and $W \sim \varepsilon$ curves obtained for the perfectly-bonded systems and those with the initial debonds are very close to each other. So, when, in extension of the debonded sample, the critical condition Equation (3) is reached at some point on the $F \sim \varepsilon$ curve, this point (taking into account the above reasoning) may be considered as that belonging to the $F \sim \varepsilon$ curve of the perfectly-bonded sample. Hence, this position may be regarded as that where the matrix detachment comes into play.

The computations give force-displacement dependence that is further converted into $\sigma \sim \varepsilon$ relationship.

3 ANALYSIS AND DISCUSSION

3.1 Strains and Stresses in Bonded Cells

The incompressibility of the matrix makes only the devictoric part of the strain tensor responsible for the storing of the elastic energy of the cell. That is why the overall picture of the strained state of the cell may be rather accurately represented by the distribution of the maximum principal strains within the matrix volume. This distribution is controlled by filler concentration and cell extension.

Strain distribution variation depending on the filler volume fraction has been examined under cell extension of 0.5%. It is shown in Figure 3 for 10, 30 and 50% filler concentrations. Here, the more strained regions are depicted qualitatively as lighter ones. From Figure 3, it may be concluded that the strain state characteristic of low filler content (10%) is close to the well-known one for a single sphere inside the infinite matrix. It is characterized by two maxima. One (point A) is positioned on the surface of the sphere at an angle of about 45° with respect to the z-axis direction. The other is in the interior of the matrix above the polar zone (point B). At higher filler content (30%), the near-surface maximum becomes more widespread (region C) while the interior one travels to the end of the cell (point D). When the filler concentration, 50%, approaches the close packing,

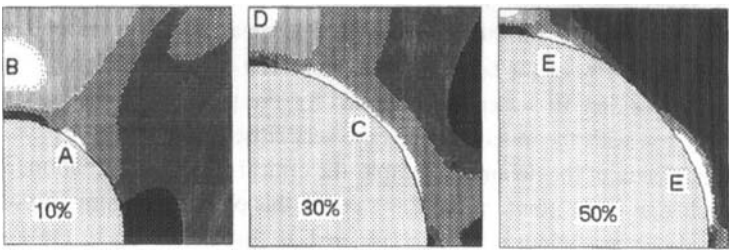

FIGURE 3 General view of the strain distributions in bonded cells at various volume filler loadings indicated on the schemes.

the near-surface maximum splits into two maxima moving apart to polar and equatorial zones of the cell (point E).

Zones containing strain concentrations represent our main interest. Their quantitative treatment has consisted in evaluation of the strain magnifications that have been represented by the ratio k

$$k = \frac{\lambda_{loc} - 1}{\lambda_{ef} - 1}, \tag{4}$$

where λ_{loc} is the local maximum stretch, and λ_{ef} is the stretch of the model cell.

The k-values have been calculated for the most strained polar zone (Fig. 4). It is seen that, even at moderate filler contents of about 0.3–0.4, the stress concentrations reach high magnitudes of the order of 5–10. They continue to grow beyond 20 at higher filler volumes, slightly increasing with extension. Therefore, cells extended to 10–20% provoke very high local strains reaching 200–400%. These values approach the ultimate ones for many elastomeric materials. Clearly, the preservation of

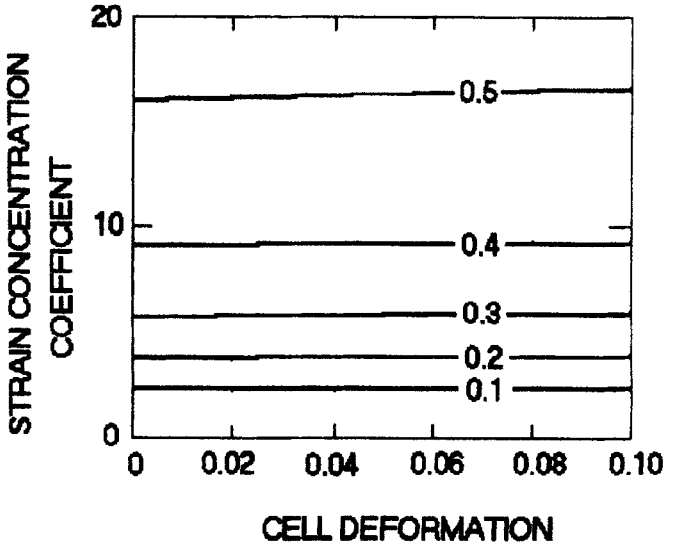

FIGURE 4 Coefficients of strain concentration as functions of the cell extension at the various filler loadings indicated on the curves.

continuity in such conditions is hardly possible. Either matrix tearing or matrix debonding will occur even at lower deformations of the cell.

It was of interest to calculate how the cell's effective modulus depends on filler volume fraction. The calculation consisted in evaluations of the energies stored in the cell at various filler contents under 0.5% extension. The relative reinforced modulus, η, was found as the ratio of the elastic energy stored in the cell with filler to that without it. Figure 5 presents the obtained modulus-concentration dependence in comparison with well-verified experimental data collected from many sources (shaded region) published in Reference [10]. The agreement between theoretical and experimental data seems to be close up to very high concentrations of more than 80% of the ultimate packing of 0.60. Of special interest is the initial part of the curve (up to 5% by volume) given as an inset in Figure 5. The initial slope came out to be 2.5 which equals the well-known Einstein's coefficient in the formula for the viscosity of suspensions. So, one can conclude that the predictive ability of the cell under consideration is rather high.

The stress state is depicted as the mean stress distribution characterizing the hydrostatic stress intensity. The typical pattern is given in Figure 6 for a cell with 30% by volume filler fraction. A strong hydrostatic extension is localized in the polar zone of the inclusion, just

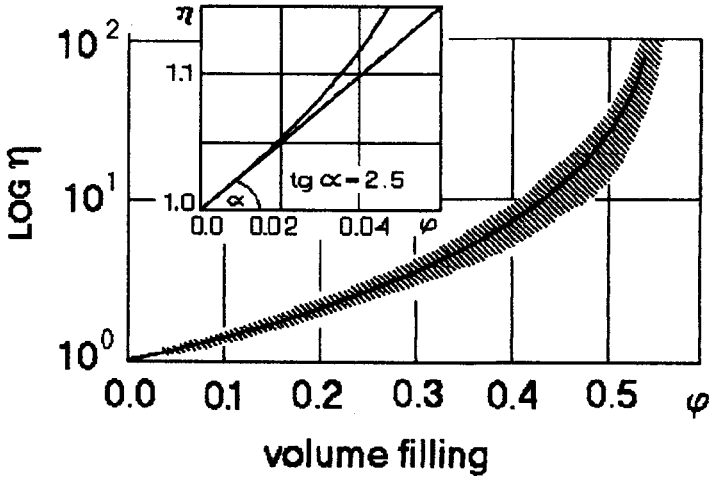

FIGURE 5 Relative modulus *versus* filler concentration for bonded cells.

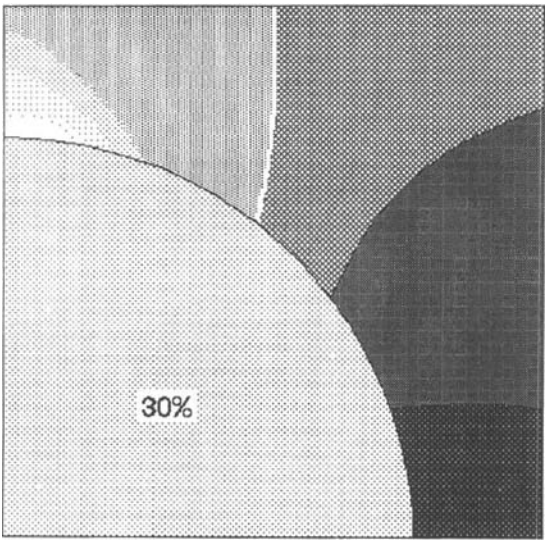

FIGURE 6 General view of the mean stress distribution for the bonded cell having 30% by volume filling. The white line divides the extended left region from the compressed right one.

where the highest strain concentration occurs. This zone may be regarded as the most predisposed to breaking-down. The general picture of the mean stress distributions remains essentially the same for other filler concentrations. It can be seen that the "participation" of the hydrostatic component in the formation of the cell resistance is markedly increasing with filler concentration due to increased matrix constraint.

Bearing in mind the geometrical peculiarities of cell distortion in tension, one can easily deduce that its ultimate radial displacements, $(u_r)_{max}$, cannot be less than the matrix width in the equatorial part of the spherical inclusion

$$(u_r)_{max} = R_C - R_S$$

where R_C is the radius of cylinder and R_S is the radius of the sphere. When, in tension, u_r tends to the inclusion's surface, the matrix widths tend to zero and corresponding perpendicular local deformations tend to infinity. This limiting transverse compression determines the corresponding ultimate longitudinal deformation, ε_b, of the cell that can be easily calculated (Fig. 7).

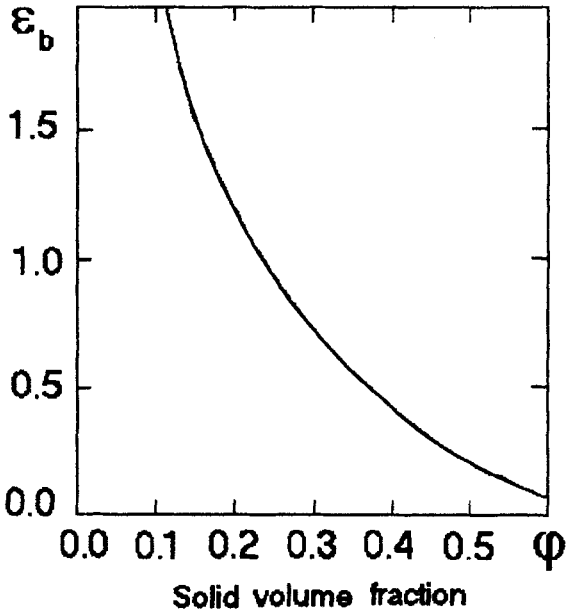

FIGURE 7 Ultimate breaking deformation, ε_b, of bonded cells as a function of the filler volume loading.

It is seen that the strongly restricted distortion characteristics of the high solid loading must inevitably lead to the matrix break-down at rather moderate cell extensions, if the system persists to remain continuous. Actual damage is supposed to occur well before reaching the limiting values shown in Figure 7.

3.2 Stresses and Strains in Debonding Cells

It is to be expected that the small debond, postulated at the pole of the inclusion, must cause a marked change in the strain and stress distribution within the matrix volume due to unloading of the most stressed part of the system. Figure 8 presents, as an example, the principal strains and mean stress distributions for a partially-debonded cell with 30% by volume filler loading. It is seen that the region above the separated zone has become weakly strained and stressed. Maximum straining now concentrates around the tip of the progressing curvilinear crack. The general character of such patterns does not change with extension and filling.

Figure 9 illustrates how the shape of the vacuole changes with extension (indicated on the curves), the point of separation being kept fixed. The diagram to the right of Figure 9 depicts the coefficients of strain concentration as a function of the cell extension. Clearly, the use of the finite element procedure provides only approximate solutions near a singularity. Nevertheless, it gives some insight into the order of magnitude of the strains computed for the grid adopted. When the detachment of the matrix from the inclusion becomes complete, strain concentration drops down to much lesser values (Fig. 10). At this point, a part of vacuole surface remains in contact with the

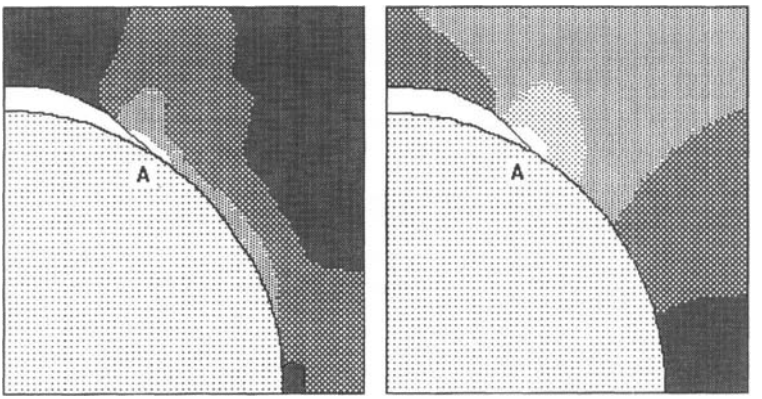

FIGURE 8 General view of the strain (a) and mean stress (b) distributions in the partially-debonded cell having 30% by volume filling.

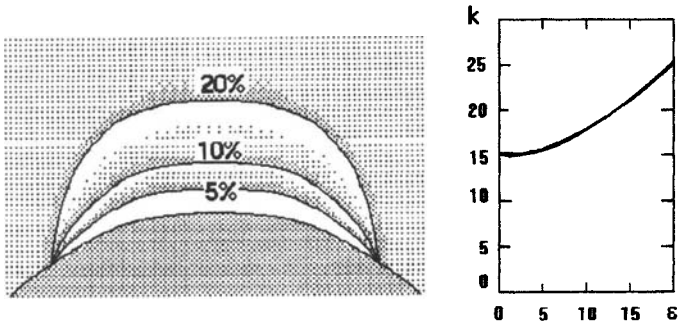

FIGURE 9 Vacuole side-views during cell extension with the fixed point of separation and coefficient of strain concentration at the crack tip as a function of the cell deformation.

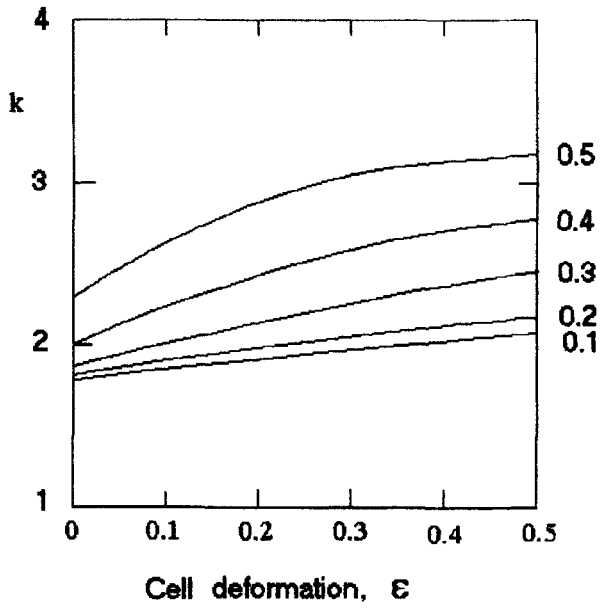

FIGURE 10 Strain concentration coefficient in the completely-detached matrix as a function of the cell deformation for various filler volume loadings indicated near the curves.

inclusion. In calculations, no friction has been assumed to exist on this contact area. The results of Figures 9 and 10 are in good agreement with the data for a rigid sphere in an infinite polymeric matrix reported in Reference [16].

It follows from Figure 10 that coefficients of strain concentration increase somewhat with cell extension in completely-debonded systems, the strain sensitivity rising with filler concentration. However, the magnitudes of those coefficients remain only a little over 3. Particulate composites, which have survived the separation stage without break-down, are able further to sustain significant deformations due to lower strain concentrations.

During matrix detachment from the inclusion, the rigidity of cells decreases from some maximum value (no debond) to some minimum one (complete debond). This drop is expected to be a function of the filler volume loading. At lower filler concentration (small sphere diameters), debonding affects the resistance of the cell slightly, a small space disturbance changing the state of the system insignificantly. In contrast,

at higher filler concentrations, when the matrix volume and the amount of stored energy become moderate, the influence of debonding is much more pronounced. Figure 11 represents upper and lower initial moduli estimations for various filler concentrations.

The shape of transition curves during the matrix separation process is exemplified by Figure 12. In these computations, the value of the debond energy, 150 J/m^2, defining a proper cohesive energy of rubber, has been used. It means that the stresses at debond gained should represent the upper limit of the debond strength of the system. Experiments show that in such events internal microscopic tears lead to a subsequent adhesive matrix separation [17]. In this regard, the debond stresses may be recognized, as well, as the upper limits of the adhesive strength. Reaching $0.2 \sim 0.3$ MPa, they turn out to be rather close to the value of the initial Young's modulus of rubber, 0.3 MPa, adopted in this investigation. This result is in good agreement with Gent's [18] assertion that the Young's modulus value may be considered as a criterion for cavitational break-down of the rubber.

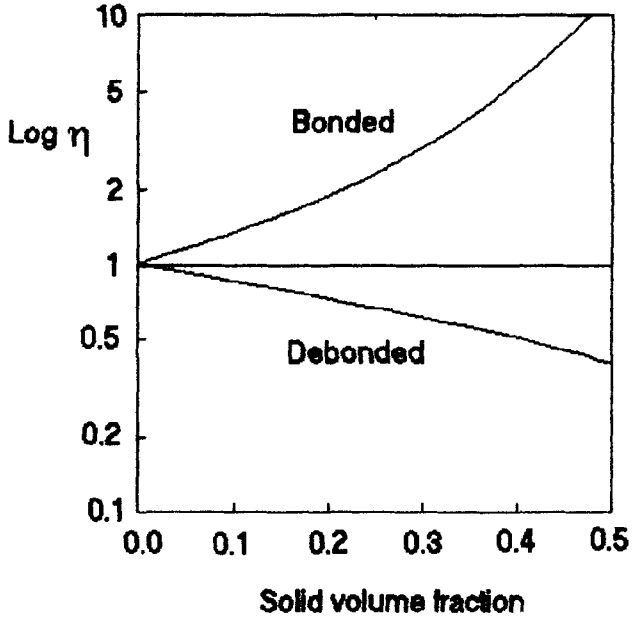

FIGURE 11 Relative moduli for perfectly-bonded and completely-debonded cells as functions of the filler volume loading.

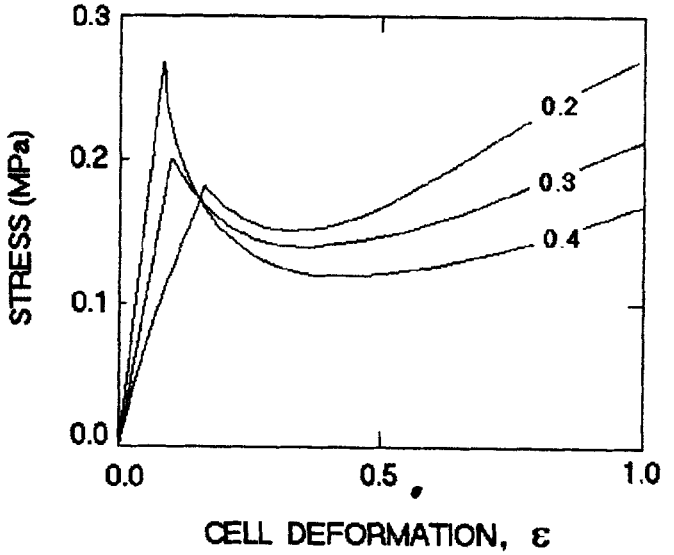

FIGURE 12 Typical shapes of tensile curves accompanied by the matrix separation for several filler volume concentrations indicated on the curves.

It is seen from Figure 12 that the separation process goes on smoothly, without local loss of stability. The transition region, from the bonded to the debonded state, that embraces not more than 80%, is followed by the extension of the entirely debonded cell.

A parameter, S, may be regarded as an evolution of some primary single structural damage. Final structural damage is represented by the rupture of the cell. So the damaging in our approach is regarded as a two-stage process in contrast to phenomenology that treats the notion of damage as a one-act process.

Calculations demonstrate that the adhesive debond energies below the tear energy examined above do not change the shapes of the transition regions, the latter going only to a lower disposition.

It is hardly possible to expect that actual tensile curves would be exact duplications of the curves computed for single cells. Obviously, the scatter of the filler concentrations in cells of actual materials, the non-uniformity of debond conditions and, even, the possible existence of the originally-debonded inclusions should inevitably lead to blurring of the detachment trajectories characteristic of individual cells. Clearly, a multitude of alternatives concerning cell non-uniformities

should produce a multitude of composite properties as is actually observed. This point merits a special examination.

5 CONCLUSIONS

1. A unit cell of a specified shape under specified loading conditions has been offered for predicting some basic properties of particulate polymeric composites.
2. The stress-strain state of the bonded and debonded cell has been investigated for various filler volume loadings, strain concentration coefficients having been calculated and examined. It has been shown that, in the bonded systems, the strain coefficients can reach several tens making the debonding process quite inevitable. On the contrary, in cells that are entirely debonded strain coefficients drop down to values of the order of 3, which accounts for the existence of large deformations after the debonding has been completed, when proper breaking strains of matrices are sufficiently large.
3. Generalized filler/modulus curves have been predicted on the basis of the single cell investigation. They proved to be in good agreement with the published experimental data over a wide range of filler concentrations.
4. The stress-strain curves of debonding cells explain well the existence of humps on the tensile curves caused exclusively by the steady process elastic separation of the matrix from the inclusions.
5. The results obtained may be regarded as basic ones for the development of advanced cell models, which could take into account time-dependency of debonding and other dissipative phenomena. They can also be used for deriving more adequate constitutive continuum relations.

Acknowledgment

The research reported in this paper has been supported by the Russian Academy of Sciences under grant 94-01-00465.

References

[1] Nicholson, D. W., "On the detachment of a rigid inclusion from an elastic matrix," *J. Adhesion* **10**, 255–260 (1979).

[2] Gent, A. N., "Detachment of an elastic matrix from a rigid spherical inclusion," *J. Mater. Sci.* **15**, 2884–2888 (1980).
[3] Paipatis, S. A., "Interfacial Phenomena and Reinforcing Mechanisms in Rubber/Carbon Black Composites," *Fiber Science and Technology* **21**, 107–124 (1984).
[4] Anderson, Lori L. and Farris, R. J., "A predictive model for the mechanical behavior of particulate composites," *Polym. Eng. Sci.* **28**, 522–527 (1988).
[5] Anderson-Vratsanos, L. and Farris, R. J., "A predictive model for the mechanical behavior of particulate composites. Part I: Model derivation," *Polym. Eng. Sci.* **33**, 1458–1465 (1993).
[6] Anderson-Vratsanos, L. and Farris, R. J., "A predictive model for the mechanical behavior of particulate composites. Part II: Comparison of model predictions to literature data," *Polym. Eng. Sci.* **33**, 1466–1474 (1993).
[7] Frankel, N. A. and Acrivos, A., "On the viscosity of a concentrated suspension of solid spheres," *Chem. Eng. Sci.* **22**, 847–853 (1967).
[8] Moshev, V. V. and Kozhevnikova, L. L., "Unit cell evolution in Structurally Damageable Particulate-Filled Elastomeric Composites under Simple Extension," *J. Adhesion* **55**(3–4) (1995).
[9] Bernal, J. D. and Mason, G., "Computation of dense random packings of hard spheres," *Nature*, No. 4754, 910–911 (1960).
[10] Chong, J. S., Christiansen, E. B. and Baer, A., "Rheology of concentrated suspensions," *J. Appl. Polym. Sci.* **15**, 2007–2021 (1971).
[11] Farris, R. J., "Prediction of the Viscosity of Multimodal Suspensions from Unimodal Viscosity Data," *Trans. Soc. Rheology* **12**(2), 281–301 (1968).
[12] Gent, A. N., "Detachment of an elastic matrix from a rigid spherical inclusion," *J. Mater. Sci.* **15**, 2884–2888 (1980).
[13] Kendall, K., "The adhesion and surface energy of elastic solids," *J. Phys. D: Appl. Phys.* **4**, 1186–1195 (1971).
[14] Gent, A. N. and Tobias, R. H., "Threshold tear strength of elastomers," *J. Polym. Sci.: Polym. Phys. Ed.* **20**, 2051–2058 (1982).
[15] Kozhevnikova, L. L., Moshev, V. V. and Rogovoy, A. A., "A continuum model for finite void growth around spherical inclusion," *Int. J. Solids Structures* **30**, 237–248 (1993).
[16] Dekkers, M. E. J. and Heikens, D., "Stress analysis near the tip of a curvilinear interfacial crack between a rigid spherical inclusion and a polymer matrix," *J. Mater. Sci.* **20**, 3865–3872 (1985).
[17] Oberth, A. E. and Bruenner, R. S., "Tear phenomena around solid inclusions in castable elastomers," *Trans. Soc. Rheol.* **9**, 165–185 (1965).
[18] Gent, A. N., "Cavitation in rubber: a cautionary tale," *Rub. Chem. Technol.* **63**(3), G49–G53 (1990).